2019

Graphene Nanoflake Uptake Mediated by Scavenger Receptors

Fatima Alnasser
University College Dublin

Valentina Castagnola
University College Dublin, valentina.castagnola@cbni.ucd.ie

Luca Boselli
University College Dublin

See next page for additional authors

Recommended Citation

Alnasser, F. et al (2019). Graphene nanoflake uptake mediated by scavenger receptors. *Nano Letters*, 19(2), pp.1260-1268. doi:10.1021/acs.nanolett.8b04820

Graphene Nanoflakes Uptake Mediated by Scavenger Receptors

Fatima Alnasser[a]‡, Valentina Castagnola[a]‡*, Luca Boselli[a], Margarita Esquivel-Gaon[a], Esen Efeoglu[b], Jennifer McIntyre[b], Hugh J. Byrne[b] and Kenneth A. Dawson[a*]

a. Centre for BioNano Interactions, School of Chemistry, University College Dublin, Belfield, Dublin 4, Ireland.
b. FOCAS Research Institute, Dublin Institute of Technology, Kevin Street, Dublin 8, Ireland
* Corresponding Authors: valentina.castagnola@cbni.ucd.ie, kenneth.a.dawson@cbni.ucd.ie, +353 (0)1 716 6928

ABSTRACT

The biological interactions of graphene have been extensively investigated over the last 10 years. However, very little is known about graphene interactions with the cell surface and how the graphene internalization process is driven and mediated by specific recognition sites at the interface with the cell. In this work, we propose a methodology to investigate direct molecular correlations between the biomolecular corona of graphene and specific cell receptors, showing that key protein recognition motifs, presented on the nanomaterial surface, can engage selectively with specific cell-receptors. We consider the case of apolipoprotein A-I, found to be very abundant in the graphene protein corona, and observe that the uptake of graphene nanoflakes is somewhat increased in cells with greatly elevated expression of scavenger receptors B1, suggesting a possible mechanism of endogenous interaction. The uptake results, obtained by flow cytometry, have been confirmed using Raman microspectroscopic mapping, exploiting the strong Raman signature of graphene.

KEYWORDS: graphene,protein corona, scavenger receptors, nanobio interactions

When nanoparticles come into contact with a biological milieu, it is typical that biomolecules derived from the environment associate to and modify their surface. This environmentally derived surface modification has been named the “biomolecular corona”.[1-2]

This idea, coupled with the privileged role of the nanoscale in endogenous biological processing, lead us to expect that synthetic objects will engage with a very broad range of living processes. The detailed nature of the initial and subsequent exchange processes by which this corona is formed depend on context and details, but typically leads to particle populations with varying biomolecular corona compositions and organization at the surface.[3-4]

Still, it is observed that typical organizations lead to several key proteins on the surface presenting receptor recognition domains and the interactions of these with target receptors are believed to form the basis of a mechanistic understanding of *in vivo* biodistribution and clearance outcomes.[5-10] It is also now believed that more complex forms of receptor-corona engagements involving scavenger and pattern recognition interactions are relevant.[11] In parallel, shape, on the nanoscale, is being investigated as a defining factor in framing biological interactions,[12-15] and therefore it can be hypothesized that this combination of shape and surface biomolecular presentation could form the basis of a broader view of biological recognition.

We stress that the biological recognition (in the context discussed here) may go considerably beyond association with a single simple recognition domain, involving complex mixtures of receptor recognition, shape, and potentially other factors yet unexplored. Nevertheless, in the short term, from a more practical point of view the ideas can be applied (on a case-by-case basis) to map explicit complex material shapes and coronas with specific endogenous bio-assemblies. This pragmatic approach, which we call nanoscale-biomimetics, seeks to identify shared features between endogenous bio-assemblies, and thereby form a link to known interactions with relevant receptors and pathways.

Among the range of nanomaterials, graphene has attracted growing attention over the last 10 years, due to its remarkable properties such as, amongst others, high surface area, inherent strength, high thermal and electrical conductivity, mechanical strength and flexibility, excellent chemical and mechanical stability and good optical transparency.[16-19] However, understanding the biological interactions of heterogeneous graphitic substances (such as fullerenes[20], carbon nanotubes[21], etc.) with cell membranes is challenging and recent reports have suggested that these materials can enter cells[22] either through direct penetration,[23] endocytosis,[15] (including clathrin-mediated endocytosis, caveolae-mediated endocytosis and macropinocytosis[24]) or phagocytic uptake.[25]

Several reports in the literature have shown *in vivo* accumulation of both micro and nano-sized graphene oxide (GO) in filter organs, especially the liver.[26-27] This is consistent with a general trend for nanoparticles and could suggest a role for receptor mediated uptake by liver-related cells. Recent progress in direct dispersion graphene in biological media has allowed the serum-derived protein corona to be explored in some detail, identifying a significant presence of apolipoprotein A-I (Apo A-I), whereas apolipoprotein B-100 (in contrast to many other common nanomaterials) was found to be nearly completely absent.[28] This might suggests that the graphene-protein complexes could interact with Scavenger Receptors B1 (SR-B1) that constitute a class of pattern-recognition receptors with a high affinity for mature high density lipoprotein (HDL), of which Apo A-I is the major protein component, and are expressed on the surface of a variety of cell types including macrophages (such as Kuppfer cells in the liver).[29-30] However, we should alert the reader to the challenges (and limitations) of working with these materials in a biological context, as implementing high levels of controls and characterization for any nanomaterial in this context is difficult,[11, 31-32] but for graphene-like materials those difficulties are magnified greatly, and even obtaining reasonable quality of dispersion requires some attention.[28]

Here, we explore the graphene-corona receptor interactions, using a HEK host-cell fusion protein platform[5] in order to over-express the receptor of interest (SR-B1 in this case) on the cell surface. We propose a protocol for the investigation of internalization mechanisms for graphene nanoflakes using flow cytometry, demonstrating that we can investigate possible links between endogenous motives presented on the graphene-based nanomaterials surface and the recognition pathways. Raman microspectroscopic mapping and Z-stack profiling was used to confirm cellular internalisation of the graphene nanoflakes.

Graphene nanoflakes exfoliated in full serum have shown a tendency to adsorb and present apolipoprotein A-I (Apo A-I) in a favourable orientation to be recognized and interact with monoclonal anti Apo A-I antibody.[28] This antibody is able to recognize amino acids 113-243 of Apo A-I of human origin, considered proxy for the HDL receptor binding domains.[33]

As mentioned previously, graphene enters the cells via different endocytosis pathways, one of which involves clathrin-mediated endocytosis or receptor-mediated endocytosis. Therefore, for the graphene nanoflakes to be internalized by these pathways, specific biomolecules or ligands need to be present and retain function on the surface of the graphene. After adsorption, these biomolecules on the surface of the graphene nanoflakes are available for interaction with cell surface receptors specifically. Once graphene nanoflakes-biomolecular complexes have interacted with cell surface receptors, cellular uptake machinery will be triggered to complete graphene flake internalization.[34] The potential recognition fragment of Apo A-I, found to be extensively present on the graphene surface, might therefore allow for the graphene binding to the SR-B1 receptor.[35-37] In a previous study, the receptor knock-down approach was investigated.[39] However, significant regulatory couplings (reciprocal up and down regulation of other scavenger receptors after knock-down of a specific scavenger receptor) was found for these conditions, leading to a difficult interpretation of the results. This issue suggested that silenced cells may not be a reliable model for this investigation, excluding the use of liver cells in the present study. Therefore, in this work, we made use of vector assisted transfection in order to overexpress specific receptors of interest on the surface of the cells. The HEK-293T cell line was chosen because of the very low endogenous expression levels of scavenger receptors, and capability for high transfection efficiency and protein production.[38]

The cells were transfected with SR-B1 receptors (see scheme in Figure 1.a) and the efficacy of the transfection was assessed by mean of HaloTag® ligand staining (as reported in Figure S1 and S2). Western blot and reverse transcription polymerase chain reaction (RT-PCR) analysis

were used as a further control for the transfection and the functionality of the overexpressed receptors was confirmed by the uptake of SR-B1 ligand acetylated LDL (see Figure S2.a-b). The receptor expression can vary widely among individual cells, creating distinct sub-populations with high, low and no receptor expression levels. Therefore, if the complete ensemble of cells is used to evaluate the graphene flake uptake levels, having heterogeneous receptor expression across the cellular population will lead to difficulties in defining a direct correlation between receptor expression and graphene nanoflake recognition. As reported in Methods, the receptors can be labelled with a fluorescent ligand (Tetramethylrhodamine, TMR) by mean of the HaloTag® function with which they are fused. The TMR fluorescence intensity can be considered an intrinsic measure of receptor expression on a cell-by-cell basis. Therefore, only a subpopulation of cells with high receptor expression levels sorted at the flow cytometry (on the basis of the TMR intensity, see Figure S2.d and S3) was considered for the following experiments. The ligand uptake was higher in the cells with high expression level of the receptors (high TMR subpopulation), therefore confirming the choice of the experimental conditions (see Figure S2.c-d and S3).

Stable graphene dispersions were produced following a previously reported protocol[28] optimized to obtain endotoxin-free material. The produced graphene nanoflakes were characterized in terms of size distribution, morphology, protein corona profile and stability overtime, in the same condition used for the *in vitro* test (see Figures S4 and S5). The measured endotoxin level after synthesis is reported in Figure S6. The SR-B1 overexpressed cells were then exposed to two different concentrations (50 μg/ml and 100 μg/ml) of exfoliated graphene. After 7 h of incubation, the cell viability was measured using MTS assay. Results showed no decrease in the cell viability after exposure to graphene nanoflakes under the conditions applied for the study, as reported in Figure S7.

The uptake was evaluated by flow cytometry using side scatter to detect the presence of graphene inside the cell. The increase in the cellular uptake of graphene was correlated to the increase in the granularity of the cells, reflected by an increase of the side scatter. This approach was previously described to estimate the uptake of metal nanoparticles and carbon based nanomaterials[40-41] and the results are reported in Figure 1.b and 1.c. The side scattering intensity was normalized by the signal obtained for the cell transfected SR-B1 not exposed to graphene, which is considered the baseline. The reported uptake is therefore presented as fold increase. The control is represented by HEK-293T cells transfected with an empty vector, therefore not presenting any overexpression of SR-B1 receptors on the surface.

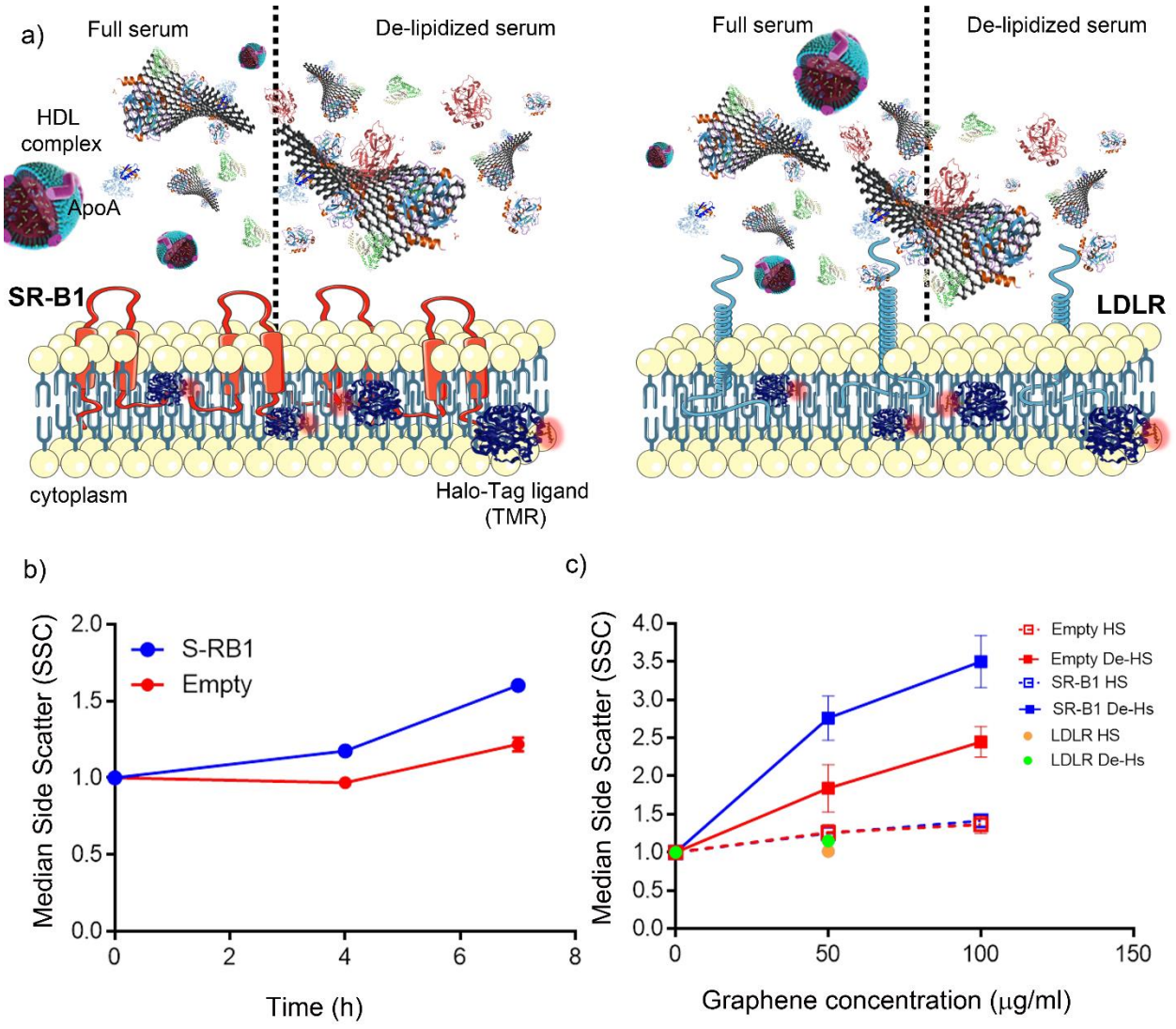

Figure 1: Evaluation of graphene uptake in transfected cells. a) Schematics of the experimental conditions showing SR-B1 and LDLR overexpressed membrane receptors in HEK-293T cells in presence of both full and delipidized serum. b) Cellular uptake as measured by side scattering in flow cytometry for SR-B1 and empty vector control transfected cells exposed to graphene nanoflakes (50 μg/ml) for 4h and 7h in 30% v/v of full human serum. c) Cellular uptake as measured by side scattering in flow cytometry for cells transfected with SR-B1 receptor exposed to graphene nanoflakes at the concentration of 50 μg/ml and 100 μg/ml in presence of both full human serum (HS) and lipoproteins depleted human serum (delipidized, De-HS). Cells transfected with empty vector were used as a control. Uptake values for LDLR transfected cells exposed to 50 μg/ml of graphene nanoflakes are also reported in presence of both full (orange dot) and delipidized (green dot) serum. For all the experiments the cells were exposed for 7h and the milieu was supplemented with 30% v/v of serum.

For all the experiments, the use of high amounts of human serum (30% v/v) aimed to set the experiment closer to an *in vivo* scenario.[42] Two particular serum conditions, illustrated in the schematic in Figure 1.a, were evaluated: full human serum and lipoproteins depleted human serum (delipidized serum). This last condition allowed to evaluate the uptake when free HDL complexes are removed from the milieu, therefore in the absence of competitive binding. Different graphene flakes sizes did not show remarkable differences therefore all the experiment here presented are referred to graphene nanoflakes called Large in Supporting Information (see Figures S4 and S8). In Figure 1.c, the effect of the competition on the receptor recognition and mediated uptake can be clearly appreciated. As a general trend, the graphene uptake is concentration dependent and it is significant for SR-B1 transfected cells in full serum (see Figure S9). However, a large increase on the uptake can be appreciated in absence of competition (see Figure 1.c and Figure S9).

As mentioned before, apolipoprotein B-100 (Apo B-100) was nearly totally absent on the graphene nanoflakes biomolecular corona.[28] Low Density Lipoprotein Receptor (LDLR) recognizes LDL complexes in which Apo B-100 is the major protein component, therefore cells transfected with LDLR were chosen as additional negative control (see scheme in Figure 1.a). After incubation with graphene nanoflakes under the same conditions used for SR-B1 transfected cells, very little uptake was found for the cells transfected with LDLR when compared to the cells transfected with empty vector (Figure 1.c).

Graphene nanoflakes are covered in a rich tapestry of proteins and ligands. For transfected cells, an unavoidable background is expected, since SR-B1 (as other scavenger receptors) also recognises a number of other ligands, and complex organizations of them, on the surface of the nanomaterials (see Figure S10). These effects cannot be fully eliminated with the proposed model. However, it was possible to observe a dominant effect conferred by the interactions with Apolipoprotein A-I that we hypothesized here.

It must be taken into account that the side scattering, used to evaluate the uptake in flow cytometry, is an intrinsically weaker signal compared to the commonly used fluorescence emission. However, biorecognition is a complex process, sensitive to any form of surface modification, including fluorescent labelling, which could disturb the interactions. Therefore, to further confirm the significance of the increased uptake for SR-B1 transfected cells, the results obtained by flow cytometry were qualitatively confirmed by Raman microspectroscopic mapping (Figure 2). Graphene possesses a very strong Raman signature due to the sp^2 hybridization (see graphene spectra in Figure S11), stronger than the intrinsic cellular signals and therefore Raman spectroscopy is considered a highly valuable tool for label free graphene detection.[43-46] Raman confocal microspectroscopy is an optical technique, and has equivalent optical resolution to Confocal Laser Scanning Fluorescence microscopy, depending on the wavelength used in each, and has previously been successfully employed for intracellular

localization of diverse carbon-based nanomaterials, also coupled with Confocal Laser Scanning Microscope (CLSM) imaging.[47]

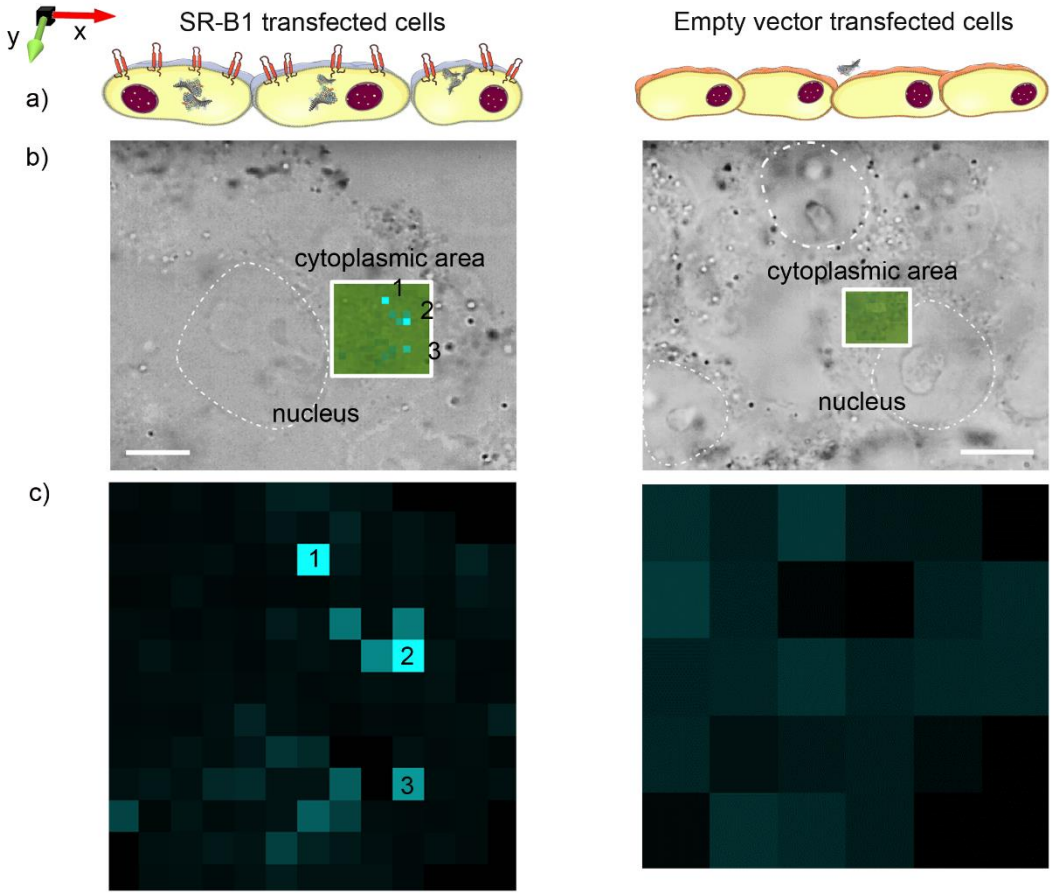

Figure 2. Raman microspectroscopic xy mapping. a) Schematic representation, b) representative optical micrographs (nucleus highlighted) and c) related Raman microspectroscopic xy mapping of the cytoplasmic areas of SR-B1 (left) and empty vector (right) transfected HEK-293T cells exposed to graphene nanoflakes (50 μg/ml for 7h). The hotspots presenting light blue colour indicate the presence of graphene nanoflakes calculated as the ratio of the intensity of G band (~1580 cm^{-1}) and amide 1 band (~1600-1700 cm^{-1}) for each recorded spectrum.

By performing xy Raman microspectroscopic mapping on random cytoplasmic areas, we were able to detect several hotspots revealing the presence of graphene, by means of its G band signal, in cells transfected with SR-B1 (Figure 2). Despite the proven stability in biological media (see Figure S4),[28] the presence of some larger graphene aggregates can be detected by optical microscopy. These aggregates, being simply deposited on the cell surface, can be displaced using the energy provided by the laser during the Raman measurements. Nevertheless, a consistent population of nanoflakes (not visible at the optical microscope) is enough stable as suspension to allow for the internalization process. In the case of cells transfected with empty vector (Figure 2) or LDL receptor (Figure S12), random scans of cytoplasmic areas never revealed graphene hotspots.

The identified hotspots in the map were subjected to Z-stack mapping to confirm that the signal detected was actually due to the presence of internalized graphene (Figure 3.a). When the closest proximity to the graphene nanoflakes is reached, graphene features dominate the Raman spectrum, compared to the cell signal. However, although graphene signal can be also detected at different depths, the ratio between the graphene peaks and cell peaks gets progressively lower. The spectra recorded at different depths in the cell cytoplasm showed typical cellular features which are partially obscured when the characteristic graphene D and G peaks start to appear, as can be seen in Figure 3.a.

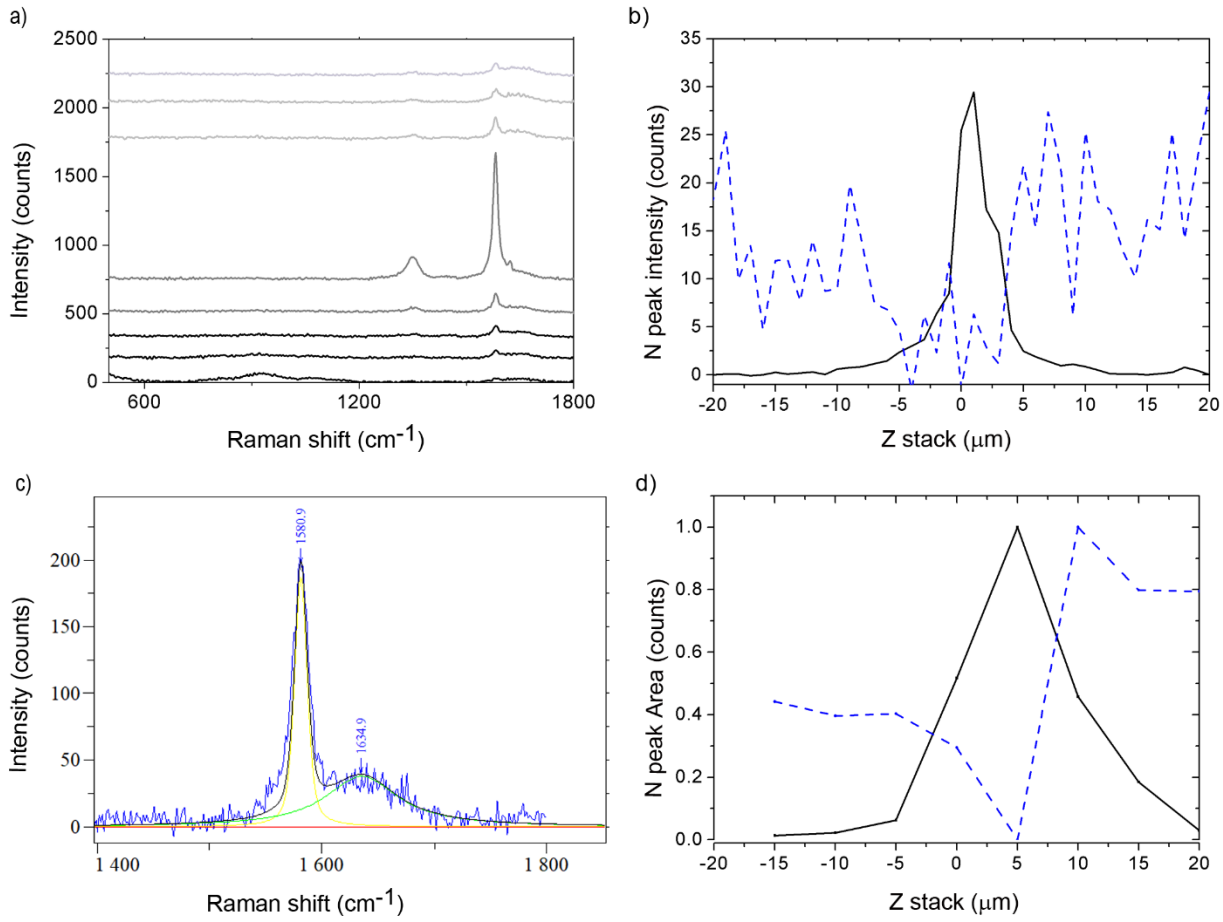

Figure 3: Z-stack analysis on hotspots in cell transfected with SR-B1 receptors and exposed to graphene nanoflakes at the concentration of 50 µg/ml for 7h**.** a). Example of Raman spectra recorded each µm from -20 µm (bottom of the dish) to 20 µm (top of the cell). Starting from -10 µm depth, the contribution from the glass substrate can be recorded around 1000 cm^{-1}, indicating that we are reaching the bottom of the dish. Spectra are offset for clarity. b) Normalized intensities for the G band (1580 cm^{-1}, black) and amide group band (1600-1700 cm^{-1}, blue dotted) over the Z-stack (measure taken every µm). c) Example of deconvolution of graphene G band and amide group band for a spectrum recorded at z = -5 µm by LabSpec 5 software analysis. The baseline was subtracted for the whole spectrum then data in the range of 1400 cm^{-1} to 1800 cm^{-1} were extracted. d) The two peaks centered respectively at 1580 cm^{-1} and ~1600 cm^{-1} at different Z levels (every 5 µm), were deconvoluted using a Gaussian-Lorentzian fitting and the so-obtained peak areas were normalized and used for the plot.

To better illustrate that the so identified graphene nanoflakes were actually inside the cell, we analysed the intensities of G band (~1580 cm^{-1}), indicative of the presence of graphene, and the protein amide I band (~1600-1700 cm^{-1}), related to the presence of proteins inside the cytoplasm (Figure 3.b). In addition, after subtraction of the spectral baselines, the two peaks of interest were fitted and deconvoluted (Figure 3.c) in order to obtain the values of area at different depths. By plotting both the normalized peak areas (Figure 3.d) as a function of focal position, it can be easily visualized how the maximum presence of graphene was detected in the middle of cell features.

Cellular features, as exemplified by the amide I band at ~1640 cm^{-1}, are clearly observed to extend over a z range of −15 ─ +20 μm, whereas the graphene related features at ~1580 cm^{-1} is clearly resolved within a region of (FWHM) 0 ─ +10 μm. Raman confocal microscopic lateral profiling at 785 nm, with a similar x100 water immersion objective, yielding a resolution of ~1μm, has previously been demonstrated to differentiate and localise nucleoli within the nuclei of cells *in vitro*,[48] and even to localise polystyrene within endosomes and lysosomes in cells.[49-50] The technique can readily be extended to depth and 3D profiling, with similar resolution.[51]

The Z-stack illustrated in Figure 3 represents an example where the cells were transfected with SR-B1 receptors and exposed to graphene nanoflakes at the concentration of 50 μg/ml for 7h. In all the SR-B1 transfected samples, it was very easy to find graphene through its Raman signature in the cytoplasmic zone, where no aggregates were visible by optical microscope. In contrast, for cells transfected with empty vector or LDLR, it was not possible to identify hotspots from the mapping and therefore to perform Z-stack analysis.

These data qualitatively confirmed the results obtained by flow cytometry, demonstrating that graphene nanoflakes were uptaken significantly more by cell transfected with SR-B1 receptors and it was possible to detect them in the intracellular space.

We first stress, once again, that our discussions are in the context of graphene in the presence of an abundance of protein, such as might be found in typical biological contexts. The interaction of graphene in the absence (or low abundance) of biomolecules is likely to be quite different, and those issues have long been discussed in the literature.[52-55] Notably, although other carbon-based nanomaterials have been found to present similar protein corona,[56-57] with the data available to date, it is premature to hypnotize a general trend based uniquely on the protein composition, considering the complexity of the recognition patterns in a competitive *in vivo* environment.

The adsorption of biomolecules on the graphene surface generates biological motifs that potentially allow for the identification of these exogenous objects, leading to partial recognition as endogenous (e.g., lipoproteins) objects and subsequent initiation of biological signalling pathways. Certainly, the system discussed here exhibits a complex combination of phenomena, including nanoflake shape and size distribution and biocorona organization, and there are likely different modes of cell-material interaction involved simultaneously. Nevertheless, it is likely that recognition motifs derived from the proteins adsorbed to the surface mediate the biological interactions, and the results presented here suggest that those interactions could be quite different for graphene from most other materials, possibly linking them to other endogenous structures processed by the liver.

Still, it is important to recognize that these are the earliest days of studies in graphene-biology, and it may be appropriate to offer very cautious and reserved judgements, on the larger scale of the implications of work such as presented here.

Graphene nanoflakes preparation and characterization

Biological dispersion of graphene nanoflakes was produced using ultrasonic exfoliation in full serum, following a protocol previously developed.[28] Special attention was devoted to the preparation of the material in endotoxin-free conditions, since it has been reported that the presence of lipopolysaccharide (LPS) can down regulate the mRNA expression of SR-B1.[58-60] Dispersions of graphene in aqueous solution were prepared by 2h ultrasonication of 50 mg of natural flake graphite (Asbury, grade 3763) 10% w/V dispersed in a solution of human serum (HS) at 50% v/v in Phosphate Buffer Saline (PBS). A bath sonicator, Fisherbrand FB11207, was used, at the frequency of 37 kHz and 100% of power. The temperature was kept around 15º C by a mixture of water and ice (70:30) in the bath, which was frequently replaced. HS off the clot was purchased from Millipore (catalogue number S1-100). The synthesis was performed in a Class 2 laminar flow hood by following all the strict precaution normally adopted during cell culture. A preventive depyrogenation of the graphite via dry heat treatment in oxygen-free conditions was performed. Briefly, the graphite was first dried from the air humidity under vacuum at 80° C (using a Schleck line) and then heated at 200° C for 4 hours. All the vials used in the synthetic and the purification procedures were endotoxin-free certified, and all the glassware were previously cleaned with aqua regia and thoroughly rinsed with endotoxin-free water. The PBS buffer (TMS-012-A, Merk Millipore) and water (TMS-011, Merk Millipore) used were both endotoxin-free certified and all the reagents (including serum) and solutions for graphene preparation were strictly opened inside the laminar flow fumehood.

For each synthesis, two main fractions were separated, following two centrifugation steps (1500 rpm for 60 min and 3000 rpm for 60 min). Finally, the samples were washed three times with fresh PBS by high speed centrifugation in order to separate unadsorbed proteins from the ones tightly bound to the surface, resulting in a stable graphene water dispersion. The

centrifugation steps for size selection were performed using an Eppendorf 5810R centrifuge. An Eppendorf 5410R centrifuge with fixed rotor 1195-A and 1.5 ml LoBind protein Eppendorf were used for the washing procedure.

The final graphene dispersions were characterized by Differential Centrifugal Sedimentation (DCS) and Transmission Electron Microscopy (TEM) as reported in Figure S4.

The DCS experiments were performed with a CPS Disc Centrifuge DC24000 (CPS Instruments). 100 μL of sample were injected in an 8-24 % PBS based sucrose gradient. Density values of 1.75 g mL^{-1}, refractive index of 2.377 and non-sphericity factor of 3 were used. The rotational speed of the disk was set to 20000 rpm.

Endotoxin level test

The Lipopolysaccharides (LPS) content in the sample was tested prior each experiment using Limulus Amebocite Lysate (LAL) chromogenic. The starting graphite powder and the exfoliated were tested by the Pierce™ LAL Chromogenic Endotoxin Quantitation Kit (88282) in BD Falcon Polystyrene Non-pyrogenic 96 well-plates (353072). 50 μL of each sample (at the concentration 100 μg/ml) was tested in duplicate following exactly the manufacturers protocol. After the reaction occurred graphite and graphene were removed by centrifugation (20000 rcf for 20 min) and only the supernatants absorbance red at the plate reader. The FDA limit for LPS is set at 0.5 EU/mL. The results are reported in Figure S6.

Cell Culture

Human Embryonic Kidney 293T (HEK-293T) cells (passage 1-25 after defrosting from liquid nitrogen; original batch from ATCC, item number CRL-3216) were cultured in Dulbecco's Modified Eagle's Medium (DMEM, high glucose, GlutaMAX™ Supplement, pyruvate) (GIBCO, 31966021), supplemented with 10% Foetal Bovine Serum (FBS,GIBCO) in a humidified chamber at 37°C under 5 % CO_2. Cells were grown in their preferred environment

and passaged three times a week, as they approached 70-80 % surface coverage. Cells were tested regularly and confirmed to be mycoplasma negative using the MycoAler Mycoplasma Detection Kit (Lonza Inc, Allendale, NJ).

Cell Transfection

HEK-293T cells were plated at a density of 104,000 cells in 1 mL of cDMEM medium in a 12 wells tissue culture plate (Cellstar® Greiner bio-one) for flow cytometry measurement and in 35 mm imaging dish with a glass bottom (ibidi) for Raman microscopy. After 24 h, cells were transfected using FuGENE 6 at a FuGENE® 6: DNA ratio of 2.5:1 and 3.5:1 for SR-B1 and LDLR respectively. Plasmid DNA was diluted in Opti-MEM medium to final concentration of 0.02 μg μL^{-1}. FuGENE® 6 reagent was then added to the diluted DNA and mixed gently by pipetting for 15 times. The transfection complex was incubated for 10 min at room temperature (RT) and 50 μl was then added dropwise to the cells and incubated for 24 h at 37 °C and 5% CO_2 before performed the uptake experiment.

The receptor is fused with HaloTag®, which can be labelled with a fluorescent ligand (Tetramethylrhodamine, TMR). TMR fluorescence intensity was used as an intrinsic measure of receptor expression on a cell-by-cell basis using flow cytometry and confocal imaging.

Exposure of cells to Graphene

To expose the cells to the graphene, the medium of the cells was replaced by 1 mL of serum-free DMEM in each well and incubated for 30 min at 37°C and 5% CO_2. The medium was then replaced by the freshly prepared graphene dispersions. Experiments were performed by diluting the concentrated graphene stock solution into 30% v/v Human Serum or 30% v/v Delipidized Human Serum at room temperature, immediately before exposure to cells. Cells were incubated with graphene nanoflakes at 37 °C and 5% CO_2 for 7 h.

Flow Cytometric Measurement of Cellular Uptake

After 7 h of exposure to graphene, the medium containing the graphene was discarded and cells were then stained with HaloTag® TMR ligand at a final concentration of 200 nM in 1 mL cDMEM and incubated for 15 min at 37 °C, 5% CO_2. After that, cells were washed once with cDMEM and twice with PBS and harvested with trypsin. Cell pellets were re-dispersed in cDMEM and placed on ice. Cell fluorescence intensity and side scatter was measured using Beckman Coulter CyAn ADP flow cytometry equipped with a 561 nm laser coupled with a 516/20 nm filter. The fluorescence intensity of TMR reflects the receptor expression level; high TMR intensity indicates high expression level of the receptors. The intensity of side scattering reflects the increase in the cell uptake of graphene. Data were analysed using Summit Software. Results are reported as the median of Side scatter of transfected cells (population of high TMR intensity) ± standard deviation of duplicates. At least 15000 cells were analyzed in each sample.

Cell Viability

The Cell viability was measured using the MTS Cell Proliferation Assay. Cells were plated 24 h prior to transfection at a density of 1000 cells/well of a 96-wells plate (Ginger) in 100 µl of cDMEM. After 24 h of transfection, the cells were exposed to 50 µg/ml of graphene for 7 h. The medium was then discarded, and cells were incubated with 20 µl of the CellTiter 96® AQueous One Solution (Promega) in 100 µl of culture medium at 37° C for 2 hours. Absorbance was measured at 490nm using a multimode microplate spectrophotometer (Varioskan Flash, Thermo Scientific, USA).

Western Blotting

Cells transfected with either SR-B1 or Empty vector were washed 3 times with PBS and lysed with radioimmunoprecipitation assay (RIPA) lysis buffer. The total protein concentration was measured using BCA assay, and all samples were normalized, and the same amount of protein

extracts was loaded for the separation on 10% sodium dodecyl sulfate polyacrylamide gel electrophoresis (SDS–PAGE) and then transferred to a PVDF membrane using Mini-PROTEAN Tetra Trans-Blot Module under a constant voltage of 100 V for 1 h. Membranes were then incubated at RT for 1 h in blocking solution of 5% skimmed milk in TBS TWEEN (150 mM NaCl, 10 mM Tris-HCl, 0.1 % Tween, pH 7.5). The membrane was then incubated with anti-SR-B1 (ab106572) and anti-GAPDH primary antibodies in 1% skimmed milk overnight at 4 °C with a gentle. Afterward, the membranes were washed 3-4 times with TBST and then incubated with anti-Goat HRP secondary antibody in 1% skimmed milk for 1 h. Then, the membranes were washed 4 times with TBST and incubated with the substrate solution for chemiluminescent reaction (ECL Western Blotting Substrate mix, Pierce) for 1 minute and visualized in Syngene G: BOX imaging system.

Reverse Transcription Polymerase Chain Reaction Analysis

RNA was extracted from sorted cells using InviTrap®Spin Cell RNA Mini Kit from Stratec (0711). The concentration and purity of the RNA samples were determined using Thermo Scientific NanoDrop 2000 spectrophotometer. The total RNA was reverse transcribed (RT) with High-Capacity cDNA Reverse Transcription Kit (Applied Biosystems™, 4368814). The expression of SR-BI and GAPDH mRNAs was determined using real-time PCR. Each cDNA sample was amplified using Power SYBR® Green PCR Master Mix (Applied Biosystems™, 4368708) on Applied Biosystems 7500 Fast Dx Real-Time PCR. GAPDH was used as an endogenous control to normalize each sample. The primers were as follows: SR-B1 forward 5'- -3'; reverse 5'- -3'; GAPDH forward 5'-ccctacaccatggagggatac-3'; reverse 5'-gcttcacccaagaagttcca-3'. Comparative CT method ($2^{-\Delta\Delta CT}$) was used to perform the calculations. The CT (Cycle Threshold) of SR-B1 was normalized with the CT of the GAPDH

to obtain its ΔCT. The value of ΔCT of SR-B1 was further normalized with the ΔCT of the control cells (i.e., untransfected cells), the result of which generated the final data set (ΔΔCT).

Raman microspectroscopic mapping and Z-stack profiling

After cell incubation with graphene and fixation with glutaraldehyde, Raman spectroscopy was performed using a Horiba-Jobin Yvon LabRam HR800 instrument equipped with a 532nm laser diode (50mW) and samples are measured in MilliQ water by using x100 water immersion objective (LUMPlanF1, Olympus, N.A. 1). The lateral spatial resolution is ~1μm, and a 100 μm confocal pinhole was used thorough out the study, resulting in a depth resolution of ~1.5μm. The scattered light is collected by the objective in a confocal geometry and is dispersed onto an air-cooled CCD detector by 600 lines/mm grating, providing approximately 1.5 cm^{-1} per pixel spectral dispersion. To avoid sample heating, Raman experiments were carried out at 10% of maximum laser power (<5 mW). The spectra were acquired for 20 seconds x3 for each spot to obtain a representative mean.

ASSOCIATED CONTENT

The Supporting Information is available free of charge on the ACS Publications website.

Figures S1-3: characterization of the transfection efficacy, Figures S4-6: characterization of the graphene nanoflakes, Figure S7: cell viability, Figure S8: uptake for different graphene nanoflakes size, Figure S9-10: statistical significance for figure 1 main text, Figures S11-12: control Raman spectra and xy mapping (PDF).

AUTHOR INFORMATION

Corresponding Author

* Corresponding Authors: valentina.castagnola@cbni.ucd.ie, kenneth.a.dawson@cbni.ucd.ie

Author Contributions

The manuscript was written through contributions of all authors. All authors have given approval to the final version of the manuscript. ‡These authors contributed equally.

ACKNOWLEDGMENT

Access to and use of the UCD Conway Facility is gratefully acknowledged. We thank Dr Laurence Fitzpatrick and Ingrid Morera for the help with confocal imaging. F.A. acknowledges the Saudi Arabia Scholarship Program (the Ministry of Education, Saudi Arabia). V. C. acknowledges the European Union Seventh Framework Programme Graphene Flagship (under grant agreement n°604391 and n°696656) and the Irish Research Council (GOIPD/2016/128). M.E-G. acknowledges the support of funding from Irish Research Council under the Enterprise Partnership PostDoctoral Fellowship Scheme 2015 (EPSPD/2015/37). L.B. acknowledges the financial support of the EU H2020 Nanofacturing project (grant agreement number 646364). K. A. D. acknowledges the Science Foundation Ireland (SFI) Principal Investigator Award (agreement number 12/IA/1422). H. J. B., E.E. and J. M. acknowledge support from Science Foundation Ireland (SFI) Principal Investigator Award PI/11/08.

REFERENCES

(1) Monopoli, M. P.; Aberg, C.; Salvati, A.; Dawson, K. A., Biomolecular coronas provide the biological identity of nanosized materials. *Nat. Nanotechnol.* **2012,** *7* (12), 779-86.

(2) Monopoli, M. P.; Walczyk, D.; Campbell, A.; Elia, G.; Lynch, I.; Baldelli Bombelli, F.; Dawson, K. A., Physical-Chemical Aspects of Protein Corona: Relevance to in Vitro and in Vivo Biological Impacts of Nanoparticles. *J. Am. Chem. Soc.* **2011,** *133* (8), 2525-2534.

(3) Lo Giudice, M. C.; Herda, L. M.; Polo, E.; Dawson, K. A., In situ characterization of nanoparticle biomolecular interactions in complex biological media by flow cytometry. *Nat. Commun.* **2016,** *7*, 13475.

(4) Kelly, P. M.; Åberg, C.; Polo, E.; O'Connell, A.; Cookman, J.; Fallon, J.; Krpetić, Ž.; Dawson, K. A., Mapping protein binding sites on the biomolecular corona of nanoparticles. *Nat. Nanotechnol.* **2015,** *10* (5), 472-479.

(5) Lara, S.; Alnasser, F.; Polo, E.; Garry, D.; Lo Giudice, M. C.; Hristov, D. R.; Rocks, L.; Salvati, A.; Yan, Y.; Dawson, K. A., Identification of Receptor Binding to the Biomolecular Corona of Nanoparticles. *ACS Nano* **2017**, *11* (2), 1884-1893.

(6) Talamini, L.; Violatto, M. B.; Cai, Q.; Monopoli, M. P.; Kantner, K.; Krpetic, Z.; Perez-Potti, A.; Cookman, J.; Garry, D.; P. Silveira, C., Influence of size and shape on the anatomical distribution of endotoxin-free gold nanoparticles. *ACS Nano* **2017**, *11* (6), 5519-5529.

(7) Huang, X.; Li, L.; Liu, T.; Hao, N.; Liu, H.; Chen, D.; Tang, F., The shape effect of mesoporous silica nanoparticles on biodistribution, clearance, and biocompatibility in vivo. *ACS Nano* **2011,** *5* (7), 5390-5399.

(8) Mortimer, G. M.; Butcher, N. J.; Musumeci, A. W.; Deng, Z. J.; Martin, D. J.; Minchin, R. F., Cryptic epitopes of albumin determine mononuclear phagocyte system clearance of nanomaterials. *ACS Nano* **2014,** *8* (4), 3357-3366.

(9) Ernsting, M. J.; Murakami, M.; Roy, A.; Li, S.-D., Factors controlling the pharmacokinetics, biodistribution and intratumoral penetration of nanoparticles. *J. Controlled Release* **2013,** *172* (3), 782-794.

(10) Sonavane, G.; Tomoda, K.; Makino, K., Biodistribution of colloidal gold nanoparticles after intravenous administration: effect of particle size. *Colloids Surf. B* **2008,** *66* (2), 274-280.

(11) Lara, S.; Perez-Potti, A.; Herda, L. M.; Adumeau, L.; Dawson, K. A.; Yan, Y., Differential Recognition of Nanoparticle Protein Corona and Modified Low Density Lipoprotein by Macrophage Receptor with Collagenous Structure. *ACS Nano* **2018**, *12* (5), 4930-4937.

(12) Castagnola, V.; Cookman, J.; De Araujo, J.; Polo, E.; Cai, Q.; Silveira, C.; Krpetić, Ž.; Yan, Y.; Boselli, L.; Dawson, K., Towards a classification strategy for complex nanostructures. *Nanoscale Horiz.* **2017**, *2* (4), 187-198.

(13) Albanese, A.; Tang, P. S.; Chan, W. C., The effect of nanoparticle size, shape, and surface chemistry on biological systems. *Annu. Rev. Biomed. Eng.* **2012,** *14*, 1-16.

(14) Chen, X.; Yan, Y.; Müllner, M.; Ping, Y.; Cui, J.; Kempe, K.; Cortez-Jugo, C.; Caruso, F., Shape-dependent activation of cytokine secretion by polymer capsules in human monocyte-derived macrophages. *Biomacromolecules* **2016,** *17* (3), 1205-1212.

(15) Vácha, R.; Martinez-Veracoechea, F. J.; Frenkel, D., Receptor-mediated endocytosis of nanoparticles of various shapes. *Nano Lett.* **2011,** *11* (12), 5391-5395.

(16) Stankovich, S.; Dikin, D. A.; Dommett, G. H. B.; Kohlhaas, K. M.; Zimney, E. J.; Stach, E. A.; Piner, R. D.; Nguyen, S. T.; Ruoff, R. S., Graphene-based composite materials. *Nature* **2006,** *442* (7100), 282-286.

(17) Balandin, A. A.; Ghosh, S.; Bao, W.; Calizo, I.; Teweldebrhan, D.; Miao, F.; Lau, C. N., Superior Thermal Conductivity of Single-Layer Graphene. *Nano Lett.* **2008,** *8* (3), 902-907.

(18) Lee, C.; Wei, X.; Kysar, J. W.; Hone, J., Measurement of the Elastic Properties and Intrinsic Strength of Monolayer Graphene. *Science* **2008,** *321* (5887), 385-388.
(19) Stoller, M. D.; Park, S.; Zhu, Y.; An, J.; Ruoff, R. S., Graphene-Based Ultracapacitors. *Nano Lett.* **2008,** *8* (10), 3498-3502.
(20) Wong-Ekkabut, J.; Baoukina, S.; Triampo, W.; Tang, I.-M.; Tieleman, D. P.; Monticelli, L., Computer simulation study of fullerene translocation through lipid membranes. *Nature Nanotechnol.* **2008,** *3* (6), 363-368.
(21) Shi, X.; von Dem Bussche, A.; Hurt, R. H.; Kane, A. B.; Gao, H., Cell entry of one-dimensional nanomaterials occurs by tip recognition and rotation. *Nature Nanotechnol.* **2011,** *6* (11), 714-719.
(22) Esquivel-Gaon, M.; Nguyen, N. H.; Sgroi, M. F.; Pullini, D.; Gili, F.; Mangherini, D.; Pruna, A. I.; Rosicka, P.; Sevcu, A.; Castagnola, V., In vitro and environmental toxicity of reduced graphene oxide as an additive in automotive lubricants. *Nanoscale* **2018,** *10* (14), 6539-6548.
(23) Zhang, Y.; Ali, S. F.; Dervishi, E.; Xu, Y.; Li, Z.; Casciano, D.; Biris, A. S., Cytotoxicity effects of graphene and single-wall carbon nanotubes in neural phaeochromocytoma-derived PC12 cells. *ACS Nano* **2010,** *4* (6), 3181-3186.
(24) Zhang, B.; Wei, P.; Zhou, Z.; Wei, T., Interactions of graphene with mammalian cells: Molecular mechanisms and biomedical insights. *Adv. Drug Delivery Rev.* **2016,** *105*, 145-162.
(25) Mu, Q.; Su, G.; Li, L.; Gilbertson, B. O.; Yu, L. H.; Zhang, Q.; Sun, Y.-P.; Yan, B., Size-dependent cell uptake of protein-coated graphene oxide nanosheets. *ACS Appl. Mater. Interfaces* **2012,** *4* (4), 2259-2266.
(26) Wang, K.; Ruan, J.; Song, H.; Zhang, J.; Wo, Y.; Guo, S.; Cui, D., Biocompatibility of graphene oxide. *Nanoscale Res. Lett.* **2011,** *6* (1), 8.
(27) Zhang, X.; Yin, J.; Peng, C.; Hu, W.; Zhu, Z.; Li, W.; Fan, C.; Huang, Q., Distribution and biocompatibility studies of graphene oxide in mice after intravenous administration. *Carbon* **2011,** *49* (3), 986-995.
(28) Castagnola, V.; Zhao, W.; Boselli, L.; Giudice, M. L.; Meder, F.; Polo, E.; Paton, K.; Backes, C.; Coleman, J.; Dawson, K., Biological recognition of graphene nanoflakes. *Nature Commun.* **2018,** *9* (1), 1577.
(29) Brown, M. S.; Goldstein, J. L., A receptor-mediated pathway for cholesterol homeostasis. *Science* **1986,** *232* (4746), 34-47.
(30) Brown, M. S.; Goldstein, J. L., Receptor-mediated endocytosis: insights from the lipoprotein receptor system. *Proc. Natl. Acad. Sci. U.S.A.* **1979,** *76* (7), 3330-3337.
(31) Reidy, B.; Haase, A.; Luch, A.; Dawson, K. A.; Lynch, I., Mechanisms of silver nanoparticle release, transformation and toxicity: a critical review of current knowledge and recommendations for future studies and applications. *Materials* **2013,** *6* (6), 2295-2350.
(32) Roebben, G.; Ramirez-Garcia, S.; Hackley, V. A.; Roesslein, M.; Klaessig, F.; Kestens, V.; Lynch, I.; Garner, C.; Rawle, A.; Elder, A., Interlaboratory comparison of size and surface charge measurements on nanoparticles prior to biological impact assessment. *J. Nanopart. Res.* **2011,** *13* (7), 2675.
(33) Allan, C. M.; Fidge, N. H.; Morrison, J. R.; Kanellos, J., Monoclonal antibodies to human apolipoprotein Al: probing the putative receptor binding domain of apolipoprotein Al. *Biochem. J.* **1993,** *290* (2), 449-455.
(34) Shang, L.; Nienhaus, K.; Nienhaus, G. U., Engineered nanoparticles interacting with cells: size matters. *J. Nanobiotechnol.* **2014,** *12* (1), 5.
(35) Kwiterovich Jr, P. O., The metabolic pathways of high-density lipoprotein, low-density lipoprotein, and triglycerides: a current review. *Am. J. Cardiol.* **2000,** *86* (12), 5-10.

(36) Rigotti, A.; Trigatti, B.; Babitt, J.; Penman, M.; Xu, S.; Krieger, M., Scavenger receptor Bl - a cell surface receptor for high density lipoprotein. *Curr. Opin. Lipidol.* **1997,** *8* (3), 181-188.
(37) Yang, X.-P.; Amar, M. J.; Vaisman, B.; Bocharov, A. V.; Vishnyakova, T. G.; Freeman, L. A.; Kurlander, R. J.; Patterson, A. P.; Becker, L. C.; Remaley, A. T., Scavenger receptor-BI is a receptor for lipoprotein(a). *J. Lipid Res.* **2013**, *54* (9), 2450-2457.
(38) Ahuja, D.; Sáenz-Robles, M. T.; Pipas, J. M., SV40 large T antigen targets multiple cellular pathways to elicit cellular transformation. *Oncogene* **2005,** *24* (52), 7729.
(39) Prapainop, K.; Miao, R.; Åberg, C.; Salvati, A.; Dawson, K. A., Reciprocal upregulation of scavenger receptors complicates interpretation of nanoparticle uptake in non-phagocytic cells. *Nanoscale* **2017,** *9* (31), 11261-11268.
(40) Zucker, R.; Daniel, K.; Massaro, E.; Karafas, S.; Degn, L.; Boyes, W., Detection of silver nanoparticles in cells by flow cytometry using light scatter and far-red fluorescence. *Cytometry, Part A* **2013,** *83* (10), 962-972.
(41) Ye, S.; Yang, P.; Cheng, K.; Zhou, T.; Wang, Y.; Hou, Z.; Jiang, Y.; Ren, L., Drp1-dependent mitochondrial fission mediates toxicity of positively charged graphene in microglia. *ACS Biomater. Sci. Eng.* **2016,** *2* (5), 722-733.
(42) Kim, J. A.; Salvati, A.; Åberg, C.; Dawson, K. A., Suppression of nanoparticle cytotoxicity approaching in vivo serum concentrations: limitations of in vitro testing for nanosafety. *Nanoscale* **2014,** *6* (23), 14180-14184.
(43) Ferrari, A. C., Raman spectroscopy of graphene and graphite: disorder, electron-phonon coupling, doping and nonadiabatic effects. *Solid State Commun.* **2007,** *143* (1), 47-57.
(44) Ferrari, A. C.; Basko, D. M., Raman spectroscopy as a versatile tool for studying the properties of graphene. *Nat. Nanotechnol.* **2013,** *8* (4), 235-246.
(45) Malard, L.; Pimenta, M.; Dresselhaus, G.; Dresselhaus, M., Raman spectroscopy in graphene. *Phys. Rep.* **2009,** *473* (5), 51-87.
(46) Girish, C. M.; Sasidharan, A.; Gowd, G. S.; Nair, S.; Koyakutty, M., Confocal Raman imaging study showing macrophage mediated biodegradation of graphene in vivo. *Adv. Healthcare Mater.* **2013,** *2* (11), 1489-1500.
(47) He, B.; Shi, Y.; Liang, Y.; Yang, A.; Fan, Z.; Yuan, L.; Zou, X.; Chang, X.; Zhang, H.; Wang, X., Single-walled carbon-nanohorns improve biocompatibility over nanotubes by triggering less protein-initiated pyroptosis and apoptosis in macrophages. *Nature Commun.* **2018,** *9* (1), 2393.
(48) Bonnier, F.; Knief, P.; Lim, B.; Meade, A.; Dorney, J.; Bhattacharya, K.; Lyng, F.; Byrne, H. J., Imaging live cells grown on a three dimensional collagen matrix using Raman microspectroscopy. *Analyst* **2010,** *135* (12), 3169-3177.
(49) Dorney, J.; Bonnier, F.; Garcia, A.; Casey, A.; Chambers, G.; Byrne, H. J., Identifying and localizing intracellular nanoparticles using Raman spectroscopy. *Analyst* **2012,** *137* (5), 1111-1119.
(50) Efeoglu, E.; Keating, M.; McIntyre, J.; Casey, A.; Byrne, H. J., Determination of nanoparticle localisation within subcellular organelles in vitro using Raman spectroscopy. *Anal. Methods* **2015,** *7* (23), 10000-10017.
(51) Majzner, K.; Kaczor, A.; Kachamakova-Trojanowska, N.; Fedorowicz, A.; Chlopicki, S.; Baranska, M., 3D confocal Raman imaging of endothelial cells and vascular wall: perspectives in analytical spectroscopy of biomedical research. *Analyst* **2013,** *138* (2), 603-610.
(52) Lesniak, A.; Fenaroli, F.; Monopoli, M. P.; Åberg, C.; Dawson, K. A.; Salvati, A., Effects of the Presence or Absence of a Protein Corona on Silica Nanoparticle Uptake and Impact on Cells. *ACS Nano* **2012,** *6* (7), 5845-5857.

(53) Mao, J.; Guo, R.; Yan, L.-T., Simulation and analysis of cellular internalization pathways and membrane perturbation for graphene nanosheets. *Biomaterials* **2014,** *35* (23), 6069-6077.
(54) Guo, R.; Mao, J.; Yan, L.-T., Computer simulation of cell entry of graphene nanosheet. *Biomaterials* **2013,** *34* (17), 4296-4301.
(55) Duan, G.; Kang, S.-g.; Tian, X.; Garate, J. A.; Zhao, L.; Ge, C.; Zhou, R., Protein corona mitigates the cytotoxicity of graphene oxide by reducing its physical interaction with cell membrane. *Nanoscale* **2015,** *7* (37), 15214-15224.
(56) Shannahan, J. H.; Brown, J. M.; Chen, R.; Ke, P. C.; Lai, X.; Mitra, S.; Witzmann, F. A., Comparison of nanotube–protein corona composition in cell culture media. *Small* **2013,** *9* (12), 2171-2181.
(57) Zhang, Y.; Wu, C.; Guo, S.; Zhang, J., Interactions of graphene and graphene oxide with proteins and peptides. *Nanotechnol. Rev.* **2013,** *2* (1), 27-45.
(58) Baranova, I.; Vishnyakova, T.; Bocharov, A.; Chen, Z.; Remaley, A. T.; Stonik, J.; Eggerman, T. L.; Patterson, A. P., Lipopolysaccharide down regulates both scavenger receptor B1 and ATP binding cassette transporter A1 in RAW cells. *Infect. and Immun.* **2002,** *70* (6), 2995-3003.
(59) Baranova, I. N.; Vishnyakova, T. G.; Bocharov, A. V.; Leelahavanichkul, A.; Kurlander, R.; Chen, Z.; Souza, A. C.; Yuen, P. S.; Star, R. A.; Csako, G., Class B scavenger receptor types I and II and CD36 mediate bacterial recognition and proinflammatory signaling induced by Escherichia coli, lipopolysaccharide, and cytosolic chaperonin 60. *The J. Immunol.* **2012,** *188* (3), 1371-1380.
(60) Hampton, R. Y.; Golenbock, D. T.; Penman, M.; Krieger, M.; Raetz, C. R., Recognition and plasma clearance of endotoxin by scavenger receptors. *Nature* **1991,** *352* (6333), 342.

TOC: